New moment magnitude scale, evidence of stress drop magnitude scaling and stochastic ground motion model for the French West Indies

S. Drouet, Marie-Paule Bouin, Fabrice Cotton

Geophysical Journal International

Geophys. J. Int. (2011) **187,** 1625–1644 doi: 10.1111/j.1365-246X.2011.05219.x

New moment magnitude scale, evidence of stress drop magnitude scaling and stochastic ground motion model for the French West Indies

Stéphane Drouet,[1] Marie-Paule Bouin[2,3] and Fabrice Cotton[1]

[1] *ISTerre, CNRS, Univ. Joseph Fourier, BP 53, 38041 Grenoble Cedex 9, France. E-mail:st_drouet@yahoo.fr*
[2] *IPGP, UMR 7154 CNRS, Sorbonne Paris Cité, Univ. Paris Diderot, 1 rue Jussieu, 75238 Paris Cedex 05, France*
[3] *Observatoire Volcanologique et Sismologique de Guadeloupe, Le Houëlmont, 97113 Gourbeyre, France*

Accepted 2011 September 3. Received 2011 July 29; in original form 2011 February 18

SUMMARY

In this study we analyse records from the 'Les Saintes' seismic sequence following the $M_w = 6.3$ earthquake of 2004 November 11, which occurred close to Guadeloupe (French West Indies). 485 earthquakes with magnitudes from 2 to 6, recorded at distances between 5 and 150 km are used. *S*-waves Fourier spectra are analysed to simultaneously determine source, path and site terms. The results show that the duration magnitude routinely estimated for the events that occurred in the region underestimate moment magnitude by 0.5 magnitude units over the whole magnitude range. From the inverted seismic moments and corner frequencies, we compute Brune's stress drops. We show that stress drops increase with increasing magnitude. The same pattern is observed on apparent stresses (i.e. the seismic energy-to-moment ratio). However, the rate of increase diminishes at high magnitudes, which is consistent with a constant stress drop model for large events. Using the results of the inversions, we perform ground motion simulations for the entire data set using the SMSIM stochastic simulation tool. The results show that a good fit ($\sigma = 0.25$) with observed data is achieved when the source is properly described by its moment magnitude and stress drop, and when site effects are taken into account. Although the magnitude-dependent stress drop model is giving better results than the constant stress drop model, the interevent variability remains high, which could suggest that stress drop depends on other parameters such as the depth of the hypocentre. In any case, the overall variability is of the same order of magnitude as usually observed in empirical ground motion prediction equations.

Key words: Fourier analysis; Earthquake ground motions; Earthquake source observations; Seismic attenuation; Site effects; South America.

1 INTRODUCTION

The Lesser Antilles arc is formed by the subduction of the American plates below the Caribbean plate in a roughly ENE direction, at a rate of about 2 cm yr^{-1} (Deng & Sykes 1995; Dixon *et al.* 1998; De Mets *et al.* 2000). It results in a high seismicity level both on the subduction interface and within the deformed Carribbean Plate (crustal events) on 100–250 km wide zone (Feuillet *et al.* 2002).

In this study we analyse crustal events of the 'Les Saintes' seismic sequence following the $M_w = 6.3$ (Harvard CMT catalogue) event that occurred on 2004 November 11 close to the Leeward Island of the eastern Carribean (Guadeloupe). The large amount of high-quality records in the area provide a very interesting data set for spectral analysis. Andrews (1986) first proposed to use multiple earthquakes recorded at the same set of stations to simultaneously invert source, path and site terms. This kind of spectral analysis has been widely used with a non-parametric (e.g. Castro *et al.* 1990; Oth *et al.* 2011) or a parametric (e.g. Edwards *et al.* 2008; Drouet *et al.* 2010) approach.

One of the first objectives of such an approach is to estimate moment magnitudes from the Fourier amplitude spectra for relatively small events. Such a moment magnitude scale is actually not available for the French Antilles and only duration magnitude is computed for events with magnitude lower than about 5.0. For the largest events, the USGS usually provides moment magnitudes from moment tensor inversions. Recent advances in the domain of strong-motion predictions show that reliable moment magnitude estimates are needed even for the small-to-moderate events to accurately predict strong ground motion (Bommer *et al.* 2007). Moreover, a homogeneous magnitude scale is required to build seismicity catalogues and recurrence distribution of earthquakes, which are the first ingredients of probabilistic seismic hazard estimations.

Another issue of the present analysis concerns the scaling of stress drop with magnitude which is still an open debate. Some authors observe an increase of seismic energy-to-moment ratio on magnitude (e.g. Abercrombie 1995; Prejean & Ellsworth 2001; Walter *et al.* 2006) or of static stress drop on magnitude (e.g. Edwards *et al.* 2008; Drouet *et al.* 2010). On the other hand, Ide & Beroza (2001) suggested that the limited frequency band available in such analyses was responsible of the apparent increase observed. Ide *et al.* (2003) reexamined the data used in Prejean & Ellsworth (2001) and found evidence that the previously observed scaling was due to a propagation effect. However, in the context of Green's function method for the simulation of earthquakes, a stress drop ratio (between the small event and the large one) greater than one is usually needed to accurately predict ground motion (e.g. Courboulex *et al.* 2010).

The origin of this scaling is, however, still not resolved and could be due to difference in the rupture process between small and large events (Brodsky & Kanamori 2001), and/or due to the effect of depth with hypocentres of larger events being deeper than those of smaller earthquakes. The 'Les Saintes' seismic sequence offers a unique opportunity to analyse this stress drop issue over a wide magnitude range.

The first part of this study is devoted to the analysis of source, path and site effects obtained from spectral analysis of the 'Les Saintes' seismic sequence records. Special attention is given to source properties. As explained later, the moment magnitudes for the six largest events are scaled with the magnitudes given by the USGS. Our results support the scaling of stress drop with magnitude. The 'Les Saintes' seismic sequence allow the analysis of earthquakes with a wide magnitude range (from 2 to 6) that all occurred in a small area. Site effects and propagation parameters are also determined and will be used for the simulation of ground motions.

Although Guadeloupe is a high seismicity region, data from large earthquakes are lacking to produce a ground motion prediction equation (GMPE) adapted to that context. Douglas *et al.* (2006a) compared recorded data and predicted ones from a number of GMPEs derived for other regions. These authors used the Scherbaum *et al.* (2004) testing procedure and showed that none of the selected GMPEs adequately predicts ground motions in Guadeloupe. One alternative consists in using data from small events to constrain ground motions for future strong events. Courboulex *et al.* (2010) used the Green's function approach to predict ground motions from the 'Les Saintes' main shock and showed that their predictions were more accurate than those estimated from GMPEs. However, this method is limited by the unconstrained ratio between the stress drops of the small event (Green's function) and the large event (simulated one).

In this study, we provide an alternative procedure for estimating ground motions in Guadeloupe, based on the stochastic simulation (SMSIM program, Boore 2003) coupled with the results of the spectral inversion presented earlier. We simulate response spectra for the entire data set using three different stress drop models (constant stress drop, model of increasing stress drop with magnitude and event-specific stress drops). We show that the interevent term standard deviation is controlled by the stress drop, and that a good description of the source including robust moment magnitude and a frequency-content indicator (stress drop) reduces interevent standard deviation.

2 DATA

On 2004 November 21, at 11:41 a magnitude $M_w = 6.3$ (Harvard global Centroid Moment Tensor catalogue, http://www.globalcmt.org/CMTsearch.html) earthquake struck the Guadeloupe (French Lesser Antilles) close to 'Les Saintes' islands. It was followed by a large number of aftershocks in the following years until now. The largest one ($M_w = 5.8$, Harvard CMT catalogue) occurred on 2005 February 14.

The main shock and its aftershocks were recorded by the French Accelerometric Network stations in Guadeloupe and Martinique, plus the accelerometric stations of the 'Conseil Général de Martinique'. The stations and data are managed by the 'Observatoire Volcanologique et Sismologique de Guadeloupe' (OVSG) in Guadeloupe and by the 'Observatoire Volcanologique et Sismologique de Martinique' (OVSM) in Martinique. All the accelerometric data are freely available at http://www-rap.obs.ujf-grenoble.fr/ (Pequegnat *et al.* 2008).

We selected all the events related to the 'Les Saintes' seismic sequence (including one foreshock) recorded by at least three stations (without restriction on magnitude) between 2004 November and 2005 December. For this time period, *P*- and *S*-wave arrival times of the accelerometric data were already picked within the CDSA project (French Antilles Seismological Data Base, Bengoubou-Valerius *et al.* 2008). From 2006 to 2009, we selected all the events with a duration magnitude determined by the OVSG greater than or equal to 3. The data set includes 485 events (see Table S1) recorded at 19 stations from Guadeloupe and 11 stations from Martinique (Fig. 1) which results in 2512 three-component records. The duration magnitudes (M_d), which are routinely estimated at the OVSG, range between 1.1 and 6.0 (for 68 events no magnitude was computed), and hypocentral distances range between 2.75 and 85.41 km for the stations in Guadeloupe and between 110.18 and 173.98 km for the stations in Martinique (Fig. 1). The list and location of the stations are indicated in Table 1.

All the records were visually inspected to identify any problem (i.e. step function within the signal, spikes etc.) and to pick *P*- and *S*-waves arrival times when necessary (i.e. for data from 2006 to 2009). Fig. 2 shows examples of data recorded at station GBGA for three different earthquakes with indication of the *P*- and *S*-waves arrival times. It shows that even very small earthquakes are well recorded. Noise Fourier spectra are computed from the beginning of the recording to the *P*-wave arrival time. *S*-waves Fourier spectra are computed from the time window starting at the *S*-wave arrival time and ending where it includes 80 per cent of the energy computed from the *S*-wave arrival time. The spectra are then smoothed using Konno & Ohmachi (1998) smoother and the two horizontal components are combined as $H = \sqrt{(\text{East} - \text{West} \times \text{North} - \text{South})}$. Finally, we only keep data with signal amplitude greater than three times the noise amplitude.

Since we are interested in very small earthquakes, the lower frequency limit is set to 0.5 Hz, where there is still significant energy in the signal for these small events. This will, in turn, limit our ability to determine robust source parameters for the largest earthquakes, especially the main shock where corner frequency is likely smaller than 0.5 Hz. However, since only four events have a duration magnitude greater than

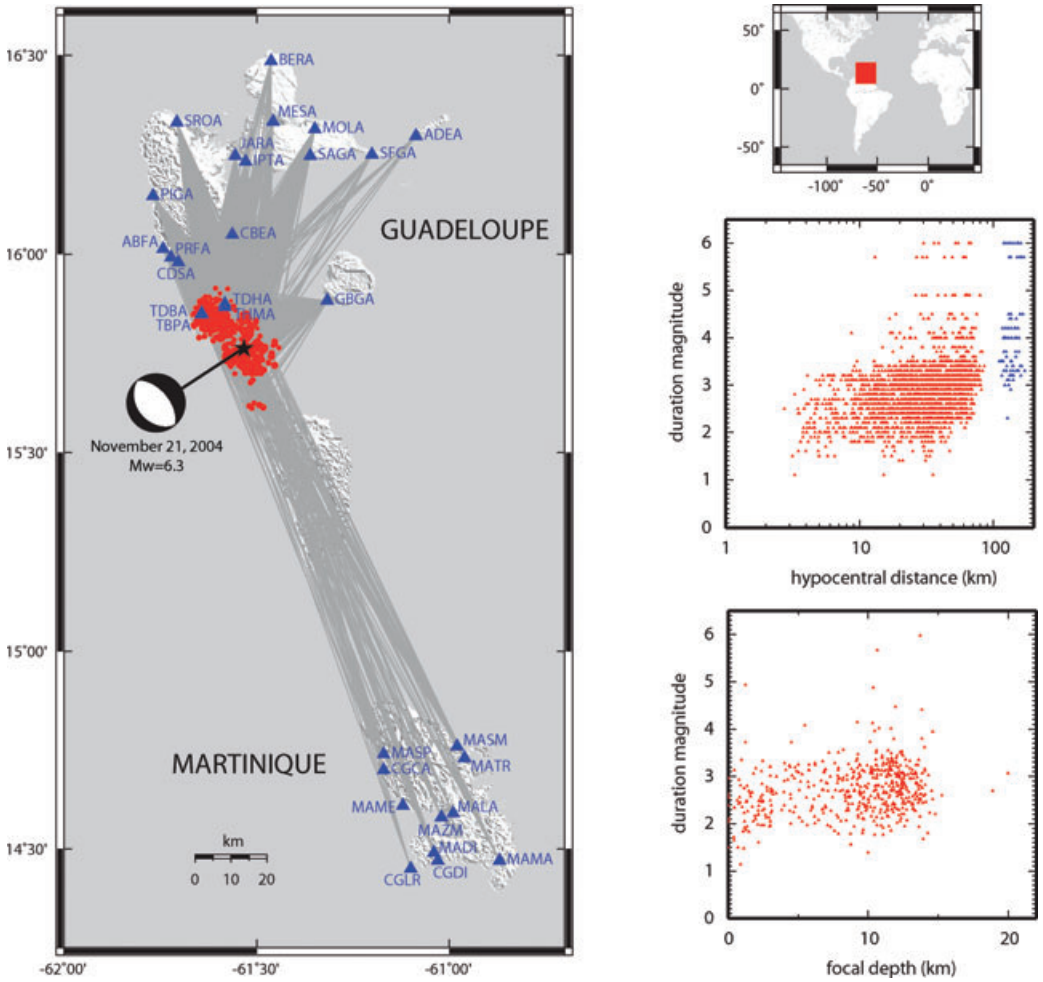

Figure 1. Left: maps of the earthquakes (red circles), stations (blue triangles) and paths (grey lines) used in this study. The location of the 2004 November 21 11:41 main shock is denoted by the black star, and its focal mechanism from Harvard CMT is shown. Right: duration magnitude—hypocentral distance distribution of the data from Guadeloupe (red triangles) and Martinique (blue triangles) and duration magnitude—focal depth distribution.

4.5 (Fig. 1), the number of good-quality data below 0.5 Hz is too small to be included. Indeed, in the inversion procedure, a large number of data at each frequency is required to simultaneously determine source, path and site parameters.

To overcome this problem, we choose to impose the moment magnitude for the largest events. This will allow us, for these events, to adjust only the corner frequency, which is possible despite the limited frequency range. The Harvard CMT catalogue contains only six events relative to the 'Les Saintes' seismic sequence (Table 2). These magnitudes will help to constrain the inversion (see the Method section).

The upper frequency limit is 30 Hz, half the Nyquist frequency of the accelerometers. Fig. 2 shows the frequency range considered for each record; clearly data below 0.5 Hz are still usable for the largest event, while for the smallest event, the lowest usable frequency is around 1.2 Hz.

3 METHOD

To simultaneously determine source, path and site effects, far-field acceleration Fourier spectra of all the records are inverted using the methodology presented in Drouet *et al.* (2008) and Drouet *et al.* (2010). The time domain convolution of the three contributions becomes a simple multiplication in the spectral domain.

$$A_{ijk}(r_{ij}, f_k) = \Omega_i(f_k) \times D_{ij}(r_{ij}, f_k) \times S_j(f_k), \tag{1}$$

where r_{ij} is the hypocentral distance from earthquake i to station j and f_k the frequency.

The source is described using the usual Brune's source model (Brune 1970, 1971).

$$\Omega_i(f_k) \sim \frac{(2\pi f_k)^2 M_{0_i}}{\left[1 + \left(\frac{f_k}{f_{c_i}}\right)^2\right]}, \tag{2}$$

where M_{0_i} is the seismic moment, and f_{c_i} the corner frequency of event i.

Table 1. Stations analysed in this study.

Name	Longitude	Latitude	Elevation (km)	Number of records
OVSG stations				
ABFA	−61.74	16.01	0.018	189
ADEA	−61.09	16.30	0.009	8
BERA	−61.46	16.49	0.031	19
CBEA	−61.56	16.05	0.029	38
CDSA	−61.70	15.98	0.420	16
GBGA	−61.32	15.88	0.009	284
IPTA	−61.53	16.23	0.020	247
JARA	−61.56	16.25	0.004	101
MESA	−61.46	16.33	0.023	76
MOLA	−61.35	16.31	0.025	89
PIGA	−61.77	16.15	0.098	223
PRFA	−61.72	15.99	0.066	378
SAGA	−61.36	16.25	0.025	14
SFGA	−61.20	16.25	0.015	15
SROA	−61.71	16.33	0.029	148
TBPA	−61.64	15.85	0.046	9
TDBA	−61.64	15.85	0.276	341
TDHA	−61.58	15.87	0.114	58
THMA	−61.58	15.87	0.012	166
OVSM stations				
CGCA	−61.17	14.70	0.015	11
CGDI	−61.03	14.47	0.005	6
CGLR	−61.10	14.45	0.050	6
MADI	−61.04	14.49	0.090	9
MALA	−60.99	14.59	0.006	6
MAMA	−60.87	14.47	0.020	9
MAME	−61.12	14.61	0.140	3
MASM	−60.98	14.76	0.040	16
MASP	−61.17	14.74	0.010	2
MATR	−60.96	14.73	0.020	16
MAZM	−61.02	14.58	0.023	9

Attenuation involves anelastic decay and geometrical spreading,

$$D_{ij}(r_{ij}, f_k) = \exp\left(-\frac{\pi r_{ij} f_k}{Q(f_k) v_S}\right) \times \frac{1}{r_{ij}^{\gamma}}, \tag{3}$$

where v_S is the average S-wave velocity along the path and $Q(f_k) = Q_0 \times f_k^{\alpha}$ is the frequency-dependent quality factor. Note that the geometrical spreading may differ from the classical r_{ij}^{-1} form through the coefficient γ. We expect γ to be greater than 1, because downward reflections from layer interfaces (e.g. Frankel 1991) and scattering (e.g. Gagnepain-Beyneix 1987) can result in a geometrical loss of energy. Some studies use a segmented geometrical decay to account for reflections on the Moho and predominance of surface waves at large distances. In our case, the limited distance range covered by the data does not allow the determination of such a complex model.

Finally, the base 10 logarithms of the Fourier spectra can be written as

$$y_{ijk} = m_{0_i} - \log_{10}\left[\left(\frac{(2\pi f_k)^2}{1 + \left(\frac{f_k}{f_{c_i}}\right)^2}\right)\right] - \gamma \log_{10}(r_{ij}) - \frac{\pi r_{ij} f_k^{1-\alpha}}{\log_e(10) Q_0 v_S} + s_{jk}, \tag{4}$$

where

$$y_{ijk} = \log_{10}\left[A_{ijk}(r_{ij}, f_k)\right], \tag{5}$$

$$m_{0_i} = \log_{10}\left[M_{0_i} \times \frac{2R_{\theta\phi}}{4\pi\rho\beta^3}\right], \tag{6}$$

$$s_{jk} = \log_{10}\left[S_j(f_k)\right], \tag{7}$$

with $R_{\theta\phi}$ the source radiation pattern, assumed to be constant ($R_{\theta\phi} = 0.55$ for S waves, Boore & Boatwright 1984), ρ the density, β the S-wave velocity of the medium at the source and v_S the S-wave velocity along the path (we assume $\beta = v_S = 3.5\ \mathrm{km\,s^{-1}}$ and $\rho = 2800\ \mathrm{kg\,m^{-3}}$). The factor 2 in eq. (6) accounts for the free surface reflection at the station assuming a quasi-vertical incidence. This is exact for *SH* and a reasonable approximation for quasi-vertical *SV* (Aki & Richards 2002).

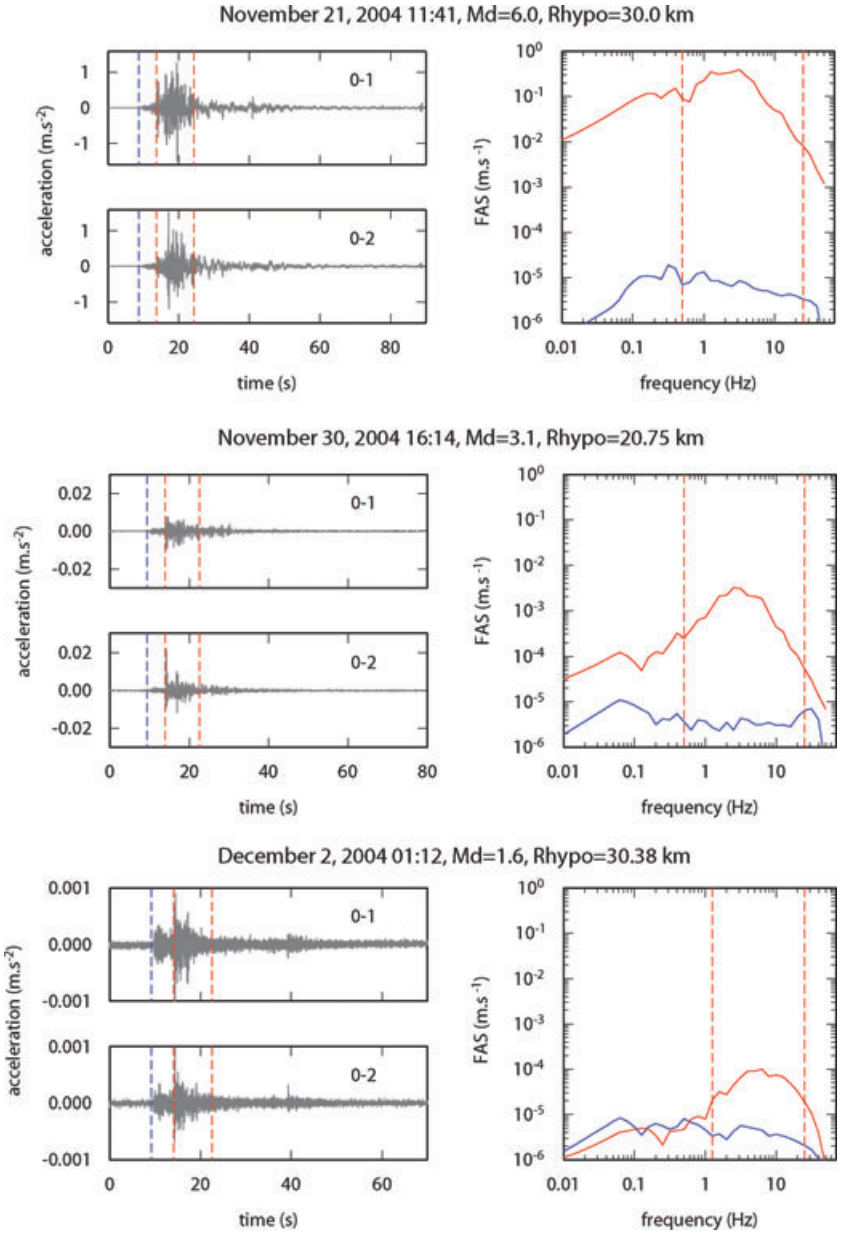

Figure 2. Examples of data for three events recorded at station GBGA. Left: horizontal acceleration time-series with *P*-wave arrival times (blue dashed line) and *S*-wave windows used to compute Fourier spectra (red dashed lines). Right: Fourier spectra for noise (blue) and signal (red) for the combined horizontal component; the usable frequency range is indicated by the dashed red lines.

Table 2. Moment magnitudes for the six largest events from the Harvard CMT catalogue (http://www.globalcmt.org/CMTsearch.html).

Events data and time	M_w
2004.11.21–11.41.00	6.3
2004.11.21–13.36.00	5.3
2004.11.21–18.53.00	5.3
2004.11.27–23.44.00	4.9
2004.12.02–14.47.00	5.0
2005.02.14–18.05.00	5.8

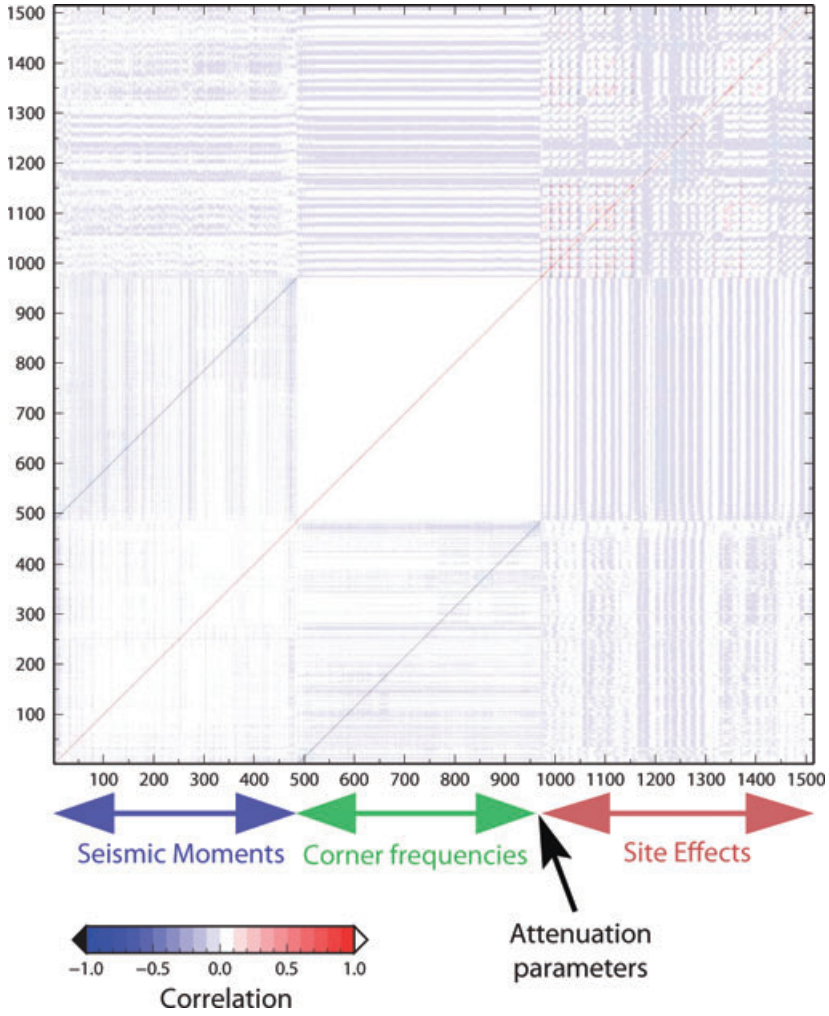

Figure 3. Correlation matrix between the inverted parameters.

There is one remaining unconstrained degree of freedom left in eq. (4) since all the seismic moments can be divided (or multiplied) by a constant value and the site terms can be multiplied (or divided) by the same value without changing the equation (Andrews 1986; Boatwright *et al.* 1991). The usual way to solve that problem is to impose that on average logarithms of site effects are null [$\sum \log_{10}(S_{jk}) = 0$]. In this study, we choose instead to impose the moment magnitudes for the six largest events.

$$m_{0_{\text{reference event}}} = \log_{10}\left[M_{0_{\text{reference event}}} \times \left(\frac{2R_{\theta\phi}}{4\pi\rho\beta^3}\right)\right] \tag{8}$$

for all of the six events from Table 2. This equation is referred to as the 'reference condition'.

The standard deviation we impose on the reference condition is small enough to ensure that the moment magnitudes for the large events will remain fixed during the inversion, allowing a robust estimation of the corner frequencies of the largest events.

We use an iterative Gauss–Newton inversion scheme, based on the derivatives of y_{ijk} with respect to the parameters, to linearize the problem at each iteration and converge to the solution (Tarantola 2004; Drouet *et al.* 2008). The standard deviation on the model parameters are computed from the covariance matrix, which is estimated after the inversion. Consequently, standard deviations presented in the following sections are probably underestimated and a better estimate could be obtained using bootstrapping but this is beyond the scope of this study. Moreover, as shown in Fig. 3 , the correlations between parameters are weak, except those theoretically expected between seismic moments and corner frequencies.

4 RESULTS

4.1 Attenuation

The data from Guadeloupe and Martinique are characterized by very different propagation paths. All the records from Guadeloupe are at distances lower than 90 km from the source and all the records from Martinique are at distances greater than 110 km from the

Table 3. Attenuation parameters determined in this study.

γ	Q_0^1	α^1	Q_0^2	α^2
One Q model				
	Guadeloupe data only			
1.088 ± 0.003	244 ± 32	0.24 ± 0.02	–	–
	Guadeloupe and Martinique data			
1.077 ± 0.001	345 ± 5	0.21 ± 0.01	–	–
Two Q models				
	Guadeloupe data		Martinique data	
1.058 ± 0.001	261 ± 12	0.16 ± 0.01	287 ± 5	0.35 ± 0.01

source. Moreover, the paths are crossing different regions and different portions of the crust, the longest paths going deeper in the crust.

We performed tests to check the influence of the data used on the propagation path parameters determination. We first used only data from Guadeloupe and then data from Guadeloupe and Martinique under two hypothesis: (1) the quality factor is the same for all the data; (2) two quality factors are defined, one for the paths towards Guadeloupe and one for the paths towards Martinique.

Table 3 shows that using all the data together with the same quality factor leads to different values for Q_0 compared to the results using only data from Guadeloupe. It also shows that using two different quality factors leads to different α values for the two categories of paths. Due to the majority of data from Guadeloupe the attenuation parameters are not changing much by the inclusion of data from Martinique. However, as shown by the test with the two quality factors, the travel paths towards Martinique are crossing less attenuating materials (higher Q_0 and α means higher quality factor), which is expected since those paths are going deeper into the crust. In the following sections, the results from the two quality factors models are shown to take into account these attenuation differences between the two kinds of paths.

4.2 Residuals

After the inversion, we compute the residuals between the observed data and the synthetic model build with the inverted parameters. The residuals distribution is shown on Fig. 4 for all the frequencies as well as for the low frequencies ($1 \leq f \leq 2$ Hz) and for the high frequencies ($15 \leq f \leq 20$ Hz). The parameters of the equivalent Gaussian distribution (mean: μ and standard deviation: σ) are also given and show a mean distribution around 0 with standard deviation almost independent of the frequency band around 0.149–0.164. The residuals are also plotted against hypocentral distance, duration magnitude and frequency in Fig. 4. These distributions and the bin average residuals do not show any trend.

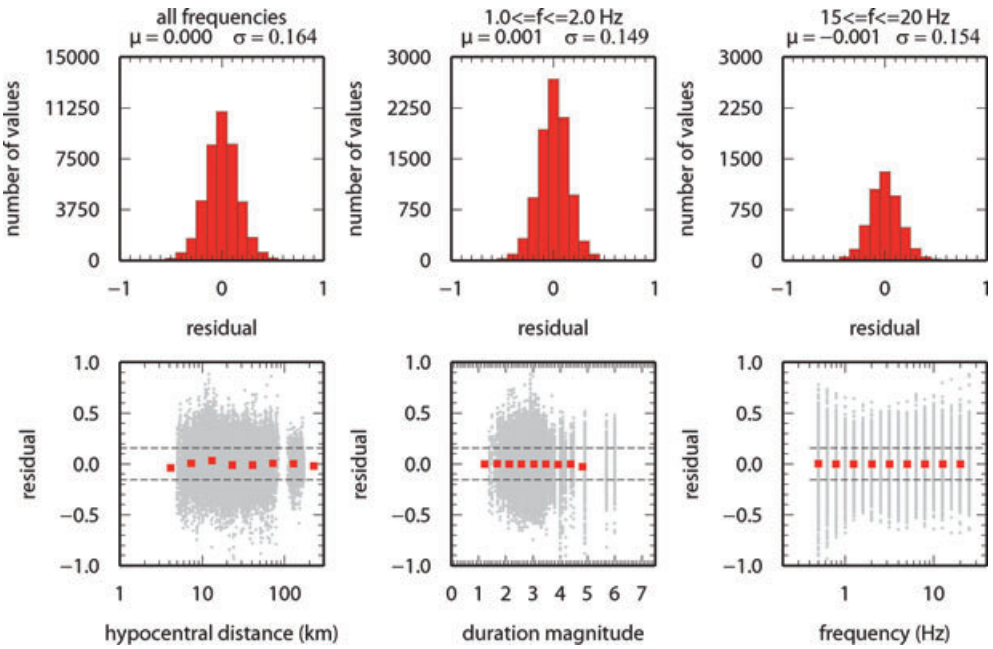

Figure 4. Top frames: residual distribution for all the frequencies and two selected frequency bands (1–2 Hz and 15–20 Hz). The parameters of the equivalent Gaussian distribution are indicated on top of each frame. Bottom frames: residuals against hypocentral distance, duration magnitude and frequency (grey triangles). The bin average residuals are also shown (red squares).

4.3 Source parameters

4.3.1 Magnitudes

Moment magnitudes are estimated from the inverted seismic moments using Hanks & Kanamori (1979) relationship

$$M_{\mathrm{w}} = \frac{\log_{10}(M_0) - 9.1}{1.5}. \tag{9}$$

They are compared with the routinely determined duration magnitude in Fig. 5 which shows that M_{d} is systematically lower than M_{w} within the magnitude range analysed, the relationship being

$$M_{\mathrm{w}} = 0.50(\pm 0.03) + 1.01(\pm 0.01) \times M_{\mathrm{d}}. \tag{10}$$

4.4 Corner frequencies and Brune's stress drop

The Brune's source model predicts a relationship between seismic moment and corner frequency, which involves the stress drop parameter $\Delta\sigma$ (Brune 1970, 1971).

$$M_0 = \frac{16}{7}\Delta\sigma \left(\frac{0.37 v_S}{f_{\mathrm{c}}}\right)^3. \tag{11}$$

Under the assumption of constant stress drop, there is a linear relationship between M_{w} [which is equivalent to $\log_{10}(M_0)$] and corner frequency $M_{\mathrm{w}} \sim -(1/3) f_{\mathrm{c}}$.

The corner frequencies are plotted against moment magnitudes in Fig. 6 , with the theoretically expected relationship for three different constant stress drop values (10^5, 10^6 and 10^7 Pa). Fig. 6 shows that stress drops are almost all lying between 1 and 500 bars (1×10^5 and 500×10^5 Pa). The linear regression shows a clear increase of stress drop with magnitude with an average value around 10×10^5 Pa for $M_{\mathrm{w}} = 2.5$ and around 100×10^5 Pa for $M_{\mathrm{w}} = 5.0$. The extrapolation of this relationship towards larger magnitudes gives a relatively large

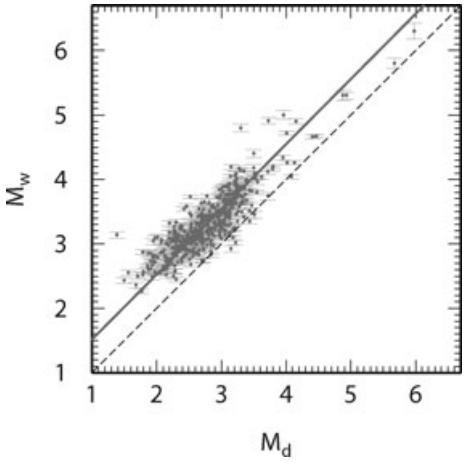

Figure 5. Comparison of the routinely determined duration magnitudes (M_{d}) and the inverted moment magnitudes (M_{w}). The regression is denoted by the grey line and the 1:1 relationship by the dashed black line.

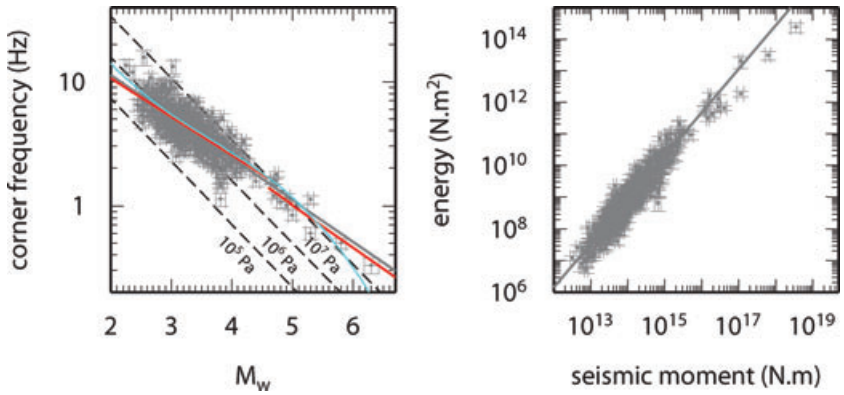

Figure 6. Left: corner frequencies against moment magnitudes. The dashed lines indicate the theoretical relationship for three different constant stress drop values: 10^5, 10^6 and 10^7 Pa. The grey line indicates the linear regression for all the events, the red lines indicate the segmented linear regression ($M_{\mathrm{w}} < 4.6$ and $M_{\mathrm{w}} \geqslant 4.6$), and the cyan line indicates the order 3 polynomial regression. Right: estimated radiated energy against seismic moment and regression line.

stress drop for the main event (493 bars) compared to the value estimated from the inverted corner frequency (263 bars). We then fit the data with a segmented regression, for events with $M_w < 4.6$ and for those with $M_w \geqslant 4.6$, and with a polynomial function of order 3. Those two regressions show a flattening of the relationship between corner frequency and moment magnitude leading to more realistic stress drop values for the larger events. This would be in agreement with the transitional model of Walter *et al.* (2006).

4.5 Radiated energy and apparent stress

The radiated energy for each event is also estimated through the integration of the squared velocity source spectra (Abercrombie 1995; Mayeda & Walter 1996). We first correct all the spectra of the same event for propagation and site effects to get source spectra, which we also convert from acceleration to velocity using the following relationship:

$$V_{ijk} = \frac{A_{ijk}}{2\pi f_k} \times r_{ij}^{\gamma} \times \exp\left(\frac{\pi r_{ij} f_k^{1-\alpha}}{Q_0 v_S}\right) \times S_j(f_k). \tag{12}$$

The average velocity source spectra over all the stations that recorded each event is squared and integrated, and the energy carried by *S* waves is estimated (Mayeda & Walter 1996).

$$E = \frac{R_{\theta\phi}}{4\pi\rho v_S^5} \times \int_{f_1}^{f_2} V(f)^2 \mathrm{d}f. \tag{13}$$

To estimate the uncertainty associated with the energy estimation, we have to compute the uncertainty linked to averaging source velocity spectra. This is done by computing the uncertainty linked to the individual spectra correction following the error propagation model:

$$\sigma = \sqrt{\left(\sigma_\gamma \times \frac{\partial \mathrm{cor}}{\partial \gamma}\right)^2 + \left(\sigma_{Q_0} \times \frac{\partial \mathrm{cor}}{\partial Q_0}\right)^2 + \left(\sigma_\alpha \times \frac{\partial \mathrm{cor}}{\partial \alpha}\right)^2 + \left(\sigma_{S_{ij}} \times \frac{\partial \mathrm{cor}}{\partial S_{ij}}\right)^2}, \tag{14}$$

which is added to the standard deviation associated with averaging the source spectra obtained at different stations.

Since most of the energy is released around the corner frequency, for small or large events the energy estimation might be biased by the frequency band limitation. Ide & Beroza (2001) computed a correction function to account for missing high frequencies in the integration that is applied to each energy estimation in this study. In the following we will assume that the *S*-waves energy represents the radiated energy. *P* waves also carry a part of the radiated energy but it is estimated to be less than 10 per cent of the total energy (Abercrombie 1995; Mayeda & Walter 1996).

Fig. 6 shows that the relationship between seismic moment and radiated energy is linear throughout the seismic moment range. For the largest events with their corner frequency outside the frequency range, the energy estimation might be biased even though we used the Ide & Beroza (2001) correction function. This could explain the departure from the linear trend for the largest events.

We also compute apparent stress

$$\sigma_a = \frac{2\mu E}{M_0}, \tag{15}$$

with $\mu = 3.4 \times 10^{10}$ Pa. Since energy might be underestimated for the largest events, apparent stresses are probably underestimated as well.

Fig. 7 shows that the scaling observed between Brune's stress drop and seismic moment also exists between apparent stress and seismic moment. One has to note, however, that the same attenuation and site terms are used in both cases, and consequently apparent stress and Brune's stress drop estimations are not completely independent. The Brune's stress drop values for the large events should not be biased,

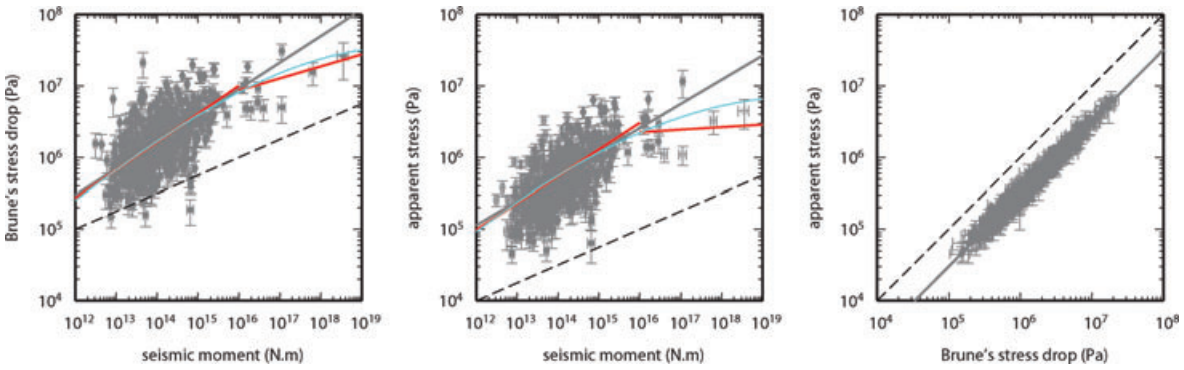

Figure 7. Left: Brune's stress drop against seismic moment. Middle: apparent stress against seismic moment for data with corner frequency well inside the frequency band (grey circles) and those with corner frequency close to the lower or upper frequency (empty grey circles). In the left and middle frames solid grey lines indicate the linear regression of the data; red lines indicate the segmented linear regression (for events with $M_w < 4.6$ and those with $M_w \geqslant 4.6$); cyan lines indicate the order 3 polynomial regression; dashed black lines indicate the scaling given by Bay *et al.* (2005) [originally developed for σ_a: $\sigma_a \propto M_0^{0.25}$ Mayeda & Walter (1996) and extrapolated to $\Delta\sigma$ assuming proportionality between $\Delta\sigma$ and σ_a Bay *et al.* (2005)]. Right: Brune's stress drop against apparent stress. Dashed black line indicates the 1:1 relationship and the grey line indicates the regression of the data.

thanks to the constraint on M_w, even though the frequency band is limited. However, one has to recall that the apparent stress drop values are underestimated for the largest events ($M_w \geqslant 4.6$). Assuming a linear relationship between stress parameters and seismic moments, the observed rate of increase is higher than that determined by Mayeda & Walter (1996) and Bay *et al.* (2005). A segmented fit for events with $M_w < 4.6$ and those with $M_w \geqslant 4.6$, or an order 3 polynomial fit show a flattening of the relationship between stresses and seismic moments towards large magnitude. This is consistent with the transitional model from Walter *et al.* (2006). Fig. 7 also shows that Brune's stress drop and apparent stress are linearly correlated.

We propose the following relationship between Brune's stress drop and seismic moment:

$$\Delta\sigma = \exp(5.9694 - 0.22431 \times \log(M_0) + 0.026126 \times (\log(M_0))^2 - 0.00034506 \times (\log(M_0))^3), \quad (16)$$

with $\Delta\sigma$ in Pa and M_0 in N m. We would like to stress that the extrapolation towards magnitudes greater than 5.5 must be used cautiously since only a limited amount of data are available in this range.

4.6 Site effects

Finally, we determine the site transfer functions for all the stations analysed in this study (Fig. 8). Due to the large amount of events recorded at each station (see Table 1) and to the limited range of backazimuths and take-off angles covered (see Fig. 1), the uncertainty on the site amplification is very small. The station with the lowest number of records (MASP, which recorded 2 events) presents also small uncertainty on the site amplification. This is probably a consequence of the large number of events, which allowed a robust estimation of source and propagation parameters.

We compare our results with H/V ratios computed using noise recordings (Douglas *et al.* 2005, 2006b, Fig. 8). The two analyses show similar resonance frequencies and similar shapes of the transfer function for most of the stations. Moreover, although there is no theoretical justification for the amplitudes to be similar, in this example they are in global agreement. At high frequency, however, there is a lack of agreement.

The stations with the flattest amplification functions and the lowest amplitudes are CGCA, IPTA, MAMA, MOLA and PIGA. Those stations can be considered as rock reference stations. Stations ABFA, SAGA and SFGA have also relatively flat transfer functions except

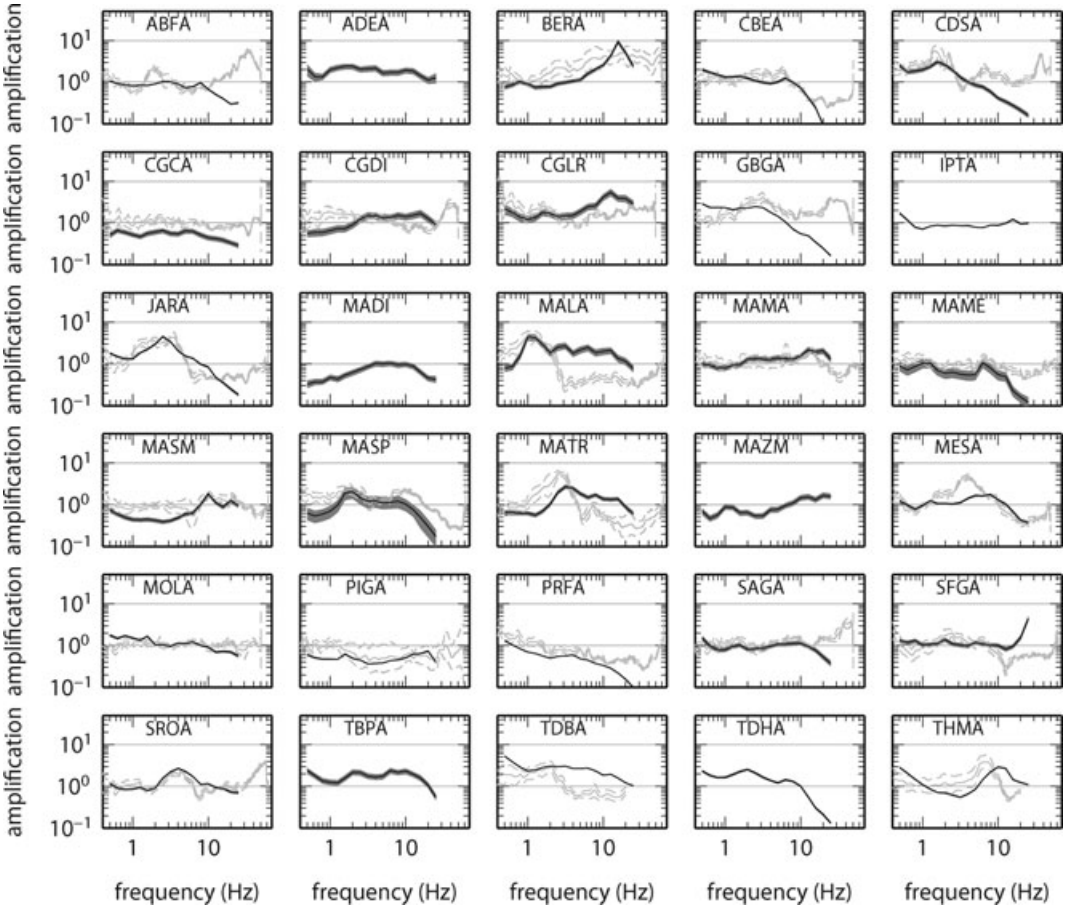

Figure 8. Site transfer functions (dark grey lines) ± one standard deviation (dark grey shaded area). H/V from noise recordings ± one standard deviation (light grey lines) from Douglas *et al.* (2005); ,2006b) are also shown.

above 10 Hz, where amplification or attenuation is observed. Station CGCA has already been identified as a potential reference station (Douglas *et al.* 2006a). These authors also classified the stations into rock and soil categories. All the reference stations determined in this study correspond to the rock category of Douglas *et al.* (2006a) as well as stations SAGA and SFGA. On the other hand, station ABFA is classified as soil in Douglas *et al.* (2006a), and many stations for which we found some amplification are classified as rock. The extreme example is station BERA for which we observe strong amplifications of about 10, around 15 Hz while, according to Douglas *et al.* (2006a), it is a rock station.

5 STOCHASTIC SIMULATIONS

The parameters determined by the inversion allow us to compute stochastic simulations using the SMSIM program (Boore 2003). The only missing piece of information to derive such a model is the strong-motion duration. Duration is defined as the time over which 5–75 per cent of the cumulative squared velocity is encapsulated (Raoof *et al.* 1999; Bay *et al.* 2003). This measure includes the source duration, which equals $1/f_c$ with f_c the corner frequency of the event, and the path duration. Fig. 9 shows the path duration against hypocentral distance estimated from the present data set. The three outliers (duration greater than 40 s) are associated to records with low signal over noise ratio. The proposed model is summarized in Table 4. Path duration of motion for Guadeloupe seems to be consistently larger than path duration for Western and Eastern North America (Atkinson & Silva 2000; Atkinson & Boore 2006).

We made simulations for all the analysed events. We used the SMSIM package developed by David Boore and freely available at: http://www.dave boore.com/software_online.htm. The required inputs are the quality factor, the geometrical spreading exponent and the path duration model for the region under investigation, as well as the site amplification functions for the recording stations. All these parameters have been previously determined in this study. The program also requires the moment magnitude and the stress drop of the event, which were also estimated and are reported in Table 5. For the stress drop, three options were tested.

(i) Use the inverted stress drop for each event as reported in Table 5.
(ii) Compute stress drop from the polynomial relationship given in eq. 16.
(iii) Use an average stress drop of 2.7×10^5 (Pa).

All the other parameters were set to standard values as in Boore (2003) and 20 time domain simulations were performed for each record. Fig. 10 compares recorded and simulated time-series (the plotted one is randomly chosen among the 20 simulations) for the $M_w = 6.3$ main shock at three stations ABFA, GBGA and MAMA. The first two are relatively close to the event (about 30 km), while MAMA is located in Martinique about 150 km away. One has to note that the simulated time-series contains only *S* waves. The amplitude and duration of the signal are reproduced quite well. Fig. 10 also compares recorded and simulated response spectra for 12 stations: eight in Guadeloupe among which four are aligned with the fault strike and four are almost perpendicular to the strike, and four stations in Martinique. One clearly sees

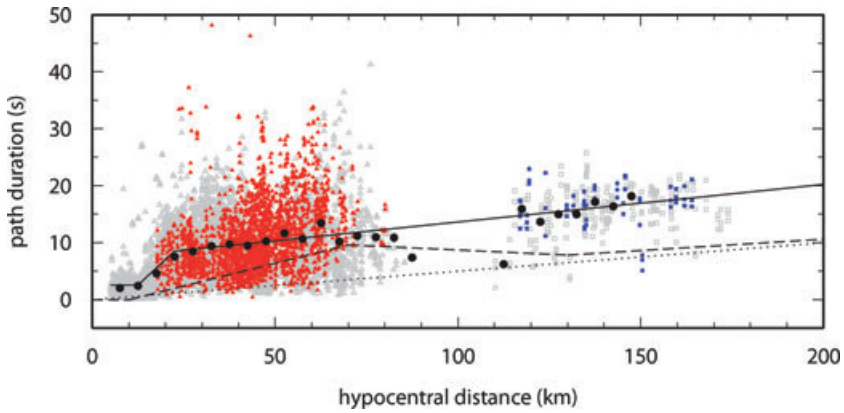

Figure 9. Path duration of shaking against hypocentral distance for rock stations (red triangles: Guadeloupe; blue squares: Martinique) and soft stations (grey triangles: Guadeloupe; grey squares: Martinique). The 5-km-binned average duration are denoted by black dots and the proposed model by the black line. The models for Western North America from Atkinson & Silva (2000) (dotted line) and for Eastern North America from Atkinson & Boore (2006) (dashed line) are also shown.

Table 4. Path duration model.

Hypocentral distance (km)	Duration (s)
0.0	0.0
5.0	2.5
12.5	2.5
22.5	8.5
> 22.5	$8.5 + 0.06 \times R_h$

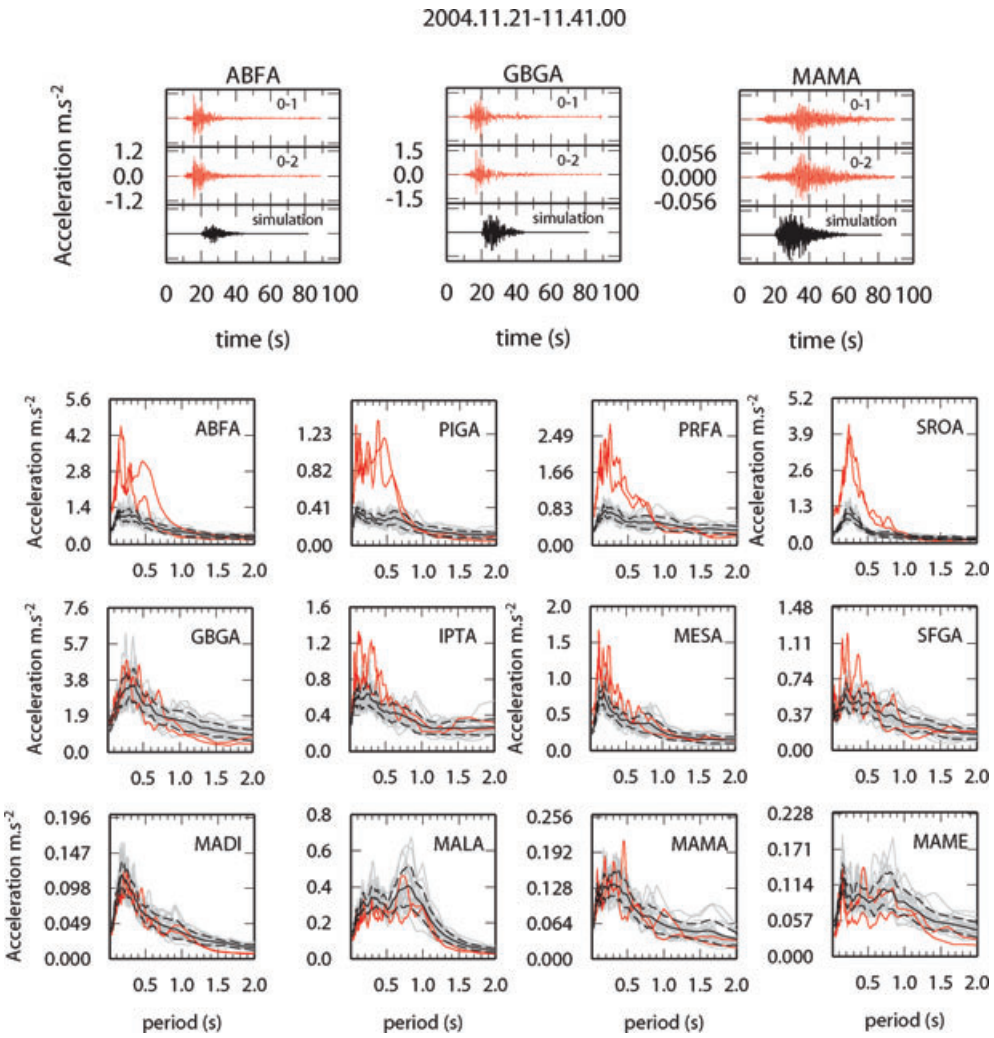

Figure 10. Time-series (red: recorded horizontal components; black: simulated horizontal component) and response spectra (red: recorded horizontal components; grey: 20 simulated horizontal components; black: average ± standard deviation simulated horizontal component) for the main shock 2004.11.21–11.41.00 $M_w = 6.3$ at a selection of stations.

that for the stations in Guadeloupe off-strike and for the stations in Martinique, simulated amplitudes are very close to recorded ones, and bumps in the response spectra due to site effects are also reproduced. However, for the four stations in Guadeloupe aligned with the faults strike, there are very high recorded amplitudes for periods below 1 s, that are not simulated. We believe that this is a directivity effect.

We compute the residuals as the differences between the logarithms of recorded and simulated response spectra. These residuals are plotted in Fig. 11 for the three hypothesis: inverted, regressed and constant stress drops. The global distributions are almost centred and the standard deviation increases with increasing frequency. At low frequency, the fit is of same quality whatever the hypothesis on stress drop. At high frequency, the standard deviation of the residuals increases rapidly from the best stress drop estimate (the inverted one) to the worst estimate (constant stress model).

To further analyse the residuals, we used the random effect model (Abrahamson & Youngs 1992) to split the residuals in an interevent term (from one event to the other) and an intraevent term (from one station to the other). The intra- and interevent residuals are shown in Fig. 12 against frequency, magnitude, distance and stress drop. While the intraevent term does not show any trend, whatever the hypothesis on stress drop, the interevent term shows a clear dependence on stress drop (and magnitude but neither are independent) when the constant stress drop model is used. A slight trend with stress drop still exists with the regressed model. It is also interesting to note the sudden increase in standard deviation of the residuals above magnitude 5 in the case where inverted stress drops are used (top middle frame of Fig. 12). The probable link of this result with a directivity effect is investigated below.

As suggested by the simulation of the main shock (Fig. 10) and by the previous results on the residuals (Fig. 12) there might be a directivity effect visible for events with magnitude above 5. To test this hypothesis, we used the information on the fault orientation from the Harvard CMT catalogue and from Courboulex *et al.* (2010) to plot the residuals as a function of the angle between the strike of the fault and the source-to-station direction (Fig. 13). This figure shows that, for most events, the residuals clearly depend on the direction from the fault

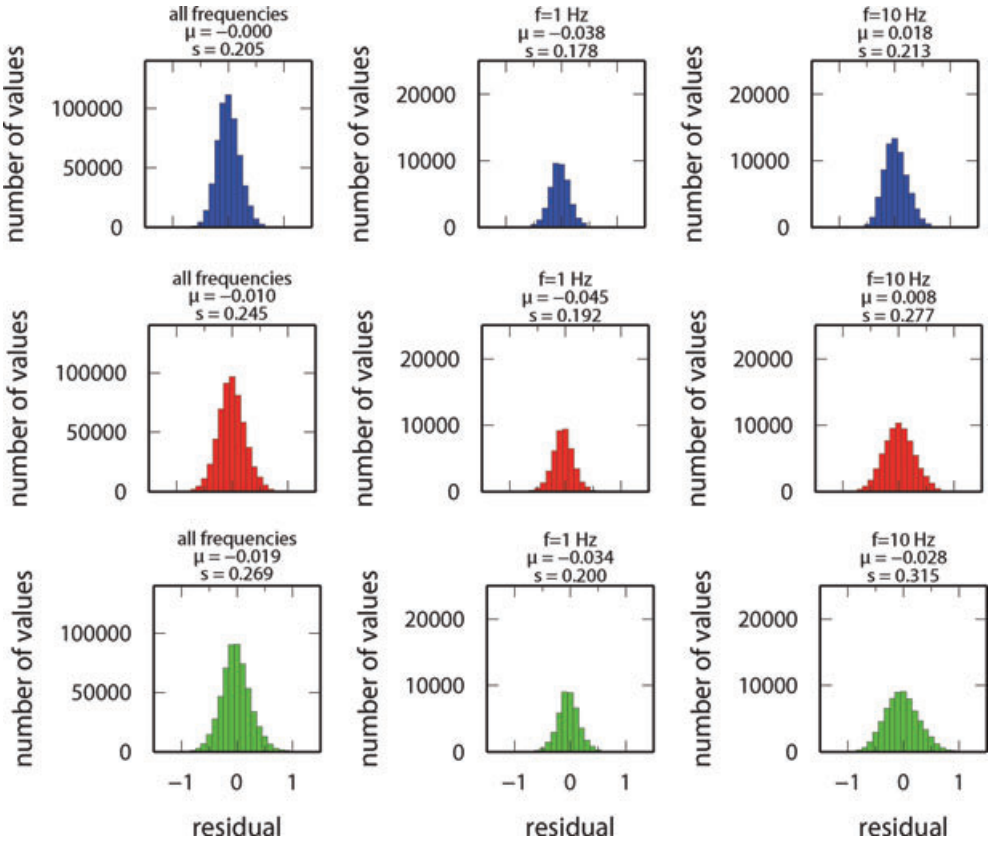

Figure 11. Distributions of the residuals (differences between the logarithms of recorded and simulated response spectra) using inverted (red), regressed (blue) and constant (green) stress drops. The parameters of the equivalent Gaussian distribution are indicated on top of each frames.

indicating larger or lower amplitudes at 0° and 180° (in both directions aligned with the fault). It seems that this effect is more pronounced for larger events. From this plot, one can then identify the direction of propagation of the rupture for each event.

6 DISCUSSION AND CONCLUSION

This study provides a set of source, path and site parameters, which reproduces the Fourier spectra in a wide range of magnitudes ($M_w = 2.5$ to 6.3) and distances ($R_{hypo} = 5$ to 140 km). The main assumptions are a Brune's source model, a homogeneous half-space and an average source radiation pattern. Complex effects like rupture directivity or site non-linearity are not taken into account. Individual standard deviation on each parameter is estimated from the covariance matrix computed after the inversion. These standard deviations are given as lower bounds since, due to configuration limitations, only a narrow range of backazimuths and take-off angles are sampled, which can contribute to low standard deviations on path and site terms. However, the large amount of data and the information redundancy also explains the low correlations and standard deviations on the parameters.

For the largest earthquakes, we had to use an *a priori* constraint. Indeed, the simultaneous analysis of small and relatively large earthquakes imposes the use of a common frequency range with signal-to-noise ratio greater than 3. Due to the scarcity of large events in the data set, the minimum frequency with enough data points for the simultaneous inversion is 0.5 Hz, which is likely above the corner frequency for the largest events. Then, inverting for both moment magnitude and corner frequency for those events is either not possible or would result in a large bias. To overcome this problem, we fixed moment magnitudes for these events using the one given by the Harvard CMT catalogue.

The attenuation properties show different patterns when one considers paths towards Guadeloupe or towards Martinique. The longer path towards Martinique are going deeper into the crust and thus are crossing less-attenuating material leading to higher Q-values for these paths. This is consistent with the usual observation of Q-values increasing with depth (Edwards *et al.* 2008). The geometrical spreading we determined is $1/R^{1.06}$. Castro *et al.* (2003) analysed 33 events in Guadeloupe and surrounding area and found two different Q models for shallow and deep events [$Q(f) = 116.8 \times f^{0.43}$ and $Q(f) = 36.3 \times f^{0.96}$, respectively], associated with two different geometrical spreading models ($1/R^{0.98 \times f^{0.26}}$ and $1/R^{0.8}$). Motazedian & Atkinson (2005) analysed around 300 earthquakes that occurred around Puerto Rico island, located about 400 km to Northwest and in a similar context as Guadeloupe (backarc of the Caribbean subduction), and found $Q(f) = 359 \times f^{0.59}$ associated with a segmented geometrical spreading: $1/R$ for $R < 75$ km, $1/R^{0.5}$ for $R > 100$ km and no geometrical attenuation between 75 and 100 km. All these models are compared in Fig. 14 . Castro *et al.*'s (2003) model for shallow events predicts a very rapid decay, faster than the results from this study, but their analysis is based on a limited data set. Castro *et al.* (2003) also found that attenuation for shallow and

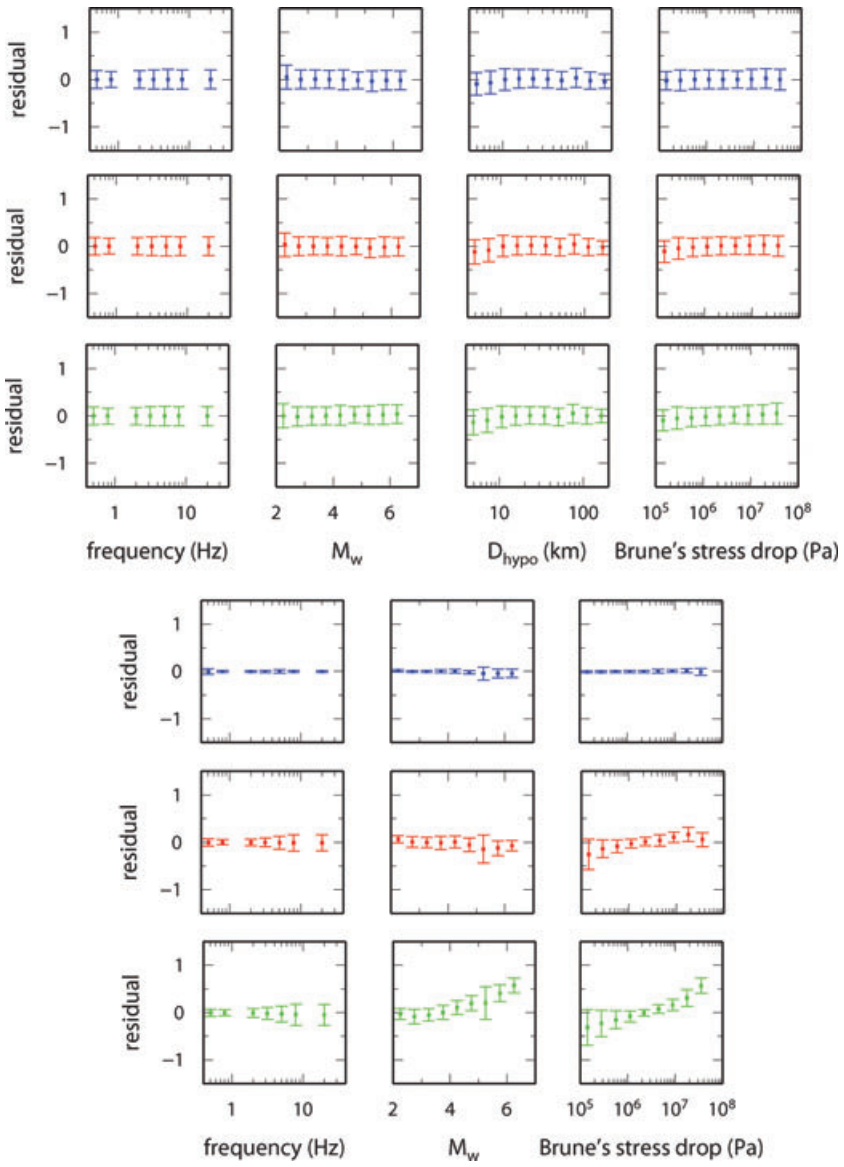

Figure 12. Top: Intraevent residuals against frequency, moment magnitude, hypocentral distance and Brune's stress drop for the three hypothesis on stress drops. Bottom: Interevent residuals against frequency, moment magnitude and Brune's stress drop again for the three hypothesis on stress drops.

deep events are significantly different, while Motazedian & Atkinson (2005) did not. For frequencies lower than 1 Hz and distances lower than 100 km, the models are similar, but at larger frequencies, they start to differ significantly. It seems that shallow events attenuate faster than deep ones. It is not clear however, whether regional differences are observed or not, since the two models for shallow events in Guadeloupe are very different although predicting a fast decay, and since the model for Puerto Rico is based on both shallow and deep events.

The inverted moment magnitudes are compared to the duration magnitudes routinely computed by the 'Observatoire Volcanologique et Sismologique de Guadeloupe'. This comparison shows a correlation with slope close to 1 between the two magnitude scales but the duration magnitudes are underestimated compared to the moment magnitudes by about 0.5 magnitude units. Drouet *et al.* (2010) found for the French metropolitan area that moment magnitudes are lower than routinely computed local magnitudes. These results have deep implications for seismic hazard assessment. Indeed, Fig. 15 shows the comparison between M_w and M_d found in this study and between M_w and M_L from Drouet *et al.* (2010) for the French Metropolitan area. Until now, seismic hazard in France is computed using the assumption $M_w = M_d$ for Guadeloupe and $M_w = M_L$ for metropolitan area.

From the moment magnitudes and corner frequencies stress drops were estimated. Our results show an increase of stress drop with magnitude. The rate of increase depends also on magnitude with a larger increase at low magnitudes and a flattening at high magnitudes, which could suggest that earthquakes with magnitude greater than 6–6.5 have an almost constant stress drop. The same observation is made from apparent stress analysis which is, however, not a completely independent measure, since the same site and attenuation corrections are used. Interestingly, Courboulex *et al.* (2010) used the empirical Green's function method to simulate ground motion using a small set of the events analysed in this study. These simulations required an estimate of the stress drop ratio between the small event (empirical Green's

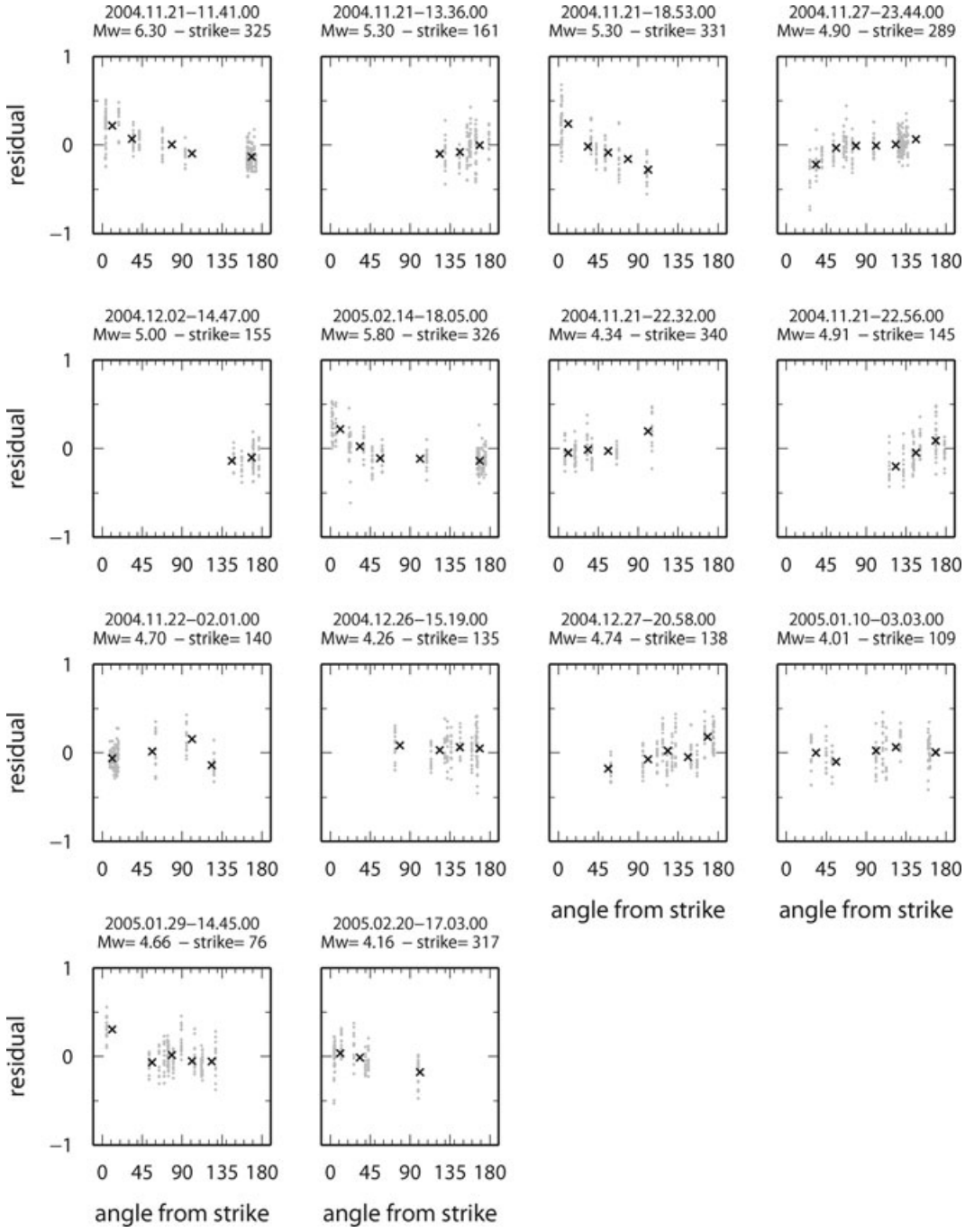

Figure 13. Residuals against the angle between the strike of the fault and the source-to-station direction for the largest events for which a fault orientation is given in the Harvard CMT catalogue or in Courboulex *et al.* (2010).

function) and the larger one. The authors estimate this ratio in the range 3–30 with the magnitude of the small events varying between 4.0 and 5.2. Our analysis gives a ratio between 0.8 and 170 for the entire data set and between 0.85 and 15 for events with magnitudes greater than 4. In this study, we mainly analysed aftershocks of the main 'Les Saintes' $M_w = 6.3$ event. Consequently, one can argue that the observed scaling of stress drop is due to low stress drops of aftershocks. However, Drouet *et al.* (2010) using the same methodology as in this paper with independent events that occurred in France metropolitan area, also found an increasing stress drop with magnitude.

This increasing stress drop with magnitude could explain part of the scaling observed in the GMPEs. However, as shown in Fig. 16, stress drops seem to depend also on depth of the earthquake which is estimated with an error of the order of 1–2 km in the studied area. Mai *et al.* (2005) have shown that rupture nucleates in the deep part of the fault and that this hypocentral depth depends on earthquake size. Assuming an increasing stress with depth, one should observe an apparent magnitude dependence of stress drop. The variability in stress drops may also result from different rupture mechanisms for small and large events (Brodsky & Kanamori 2001; Ben-Zion & Zhu 2002) or from various fault maturities (Radiguet *et al.* 2009).

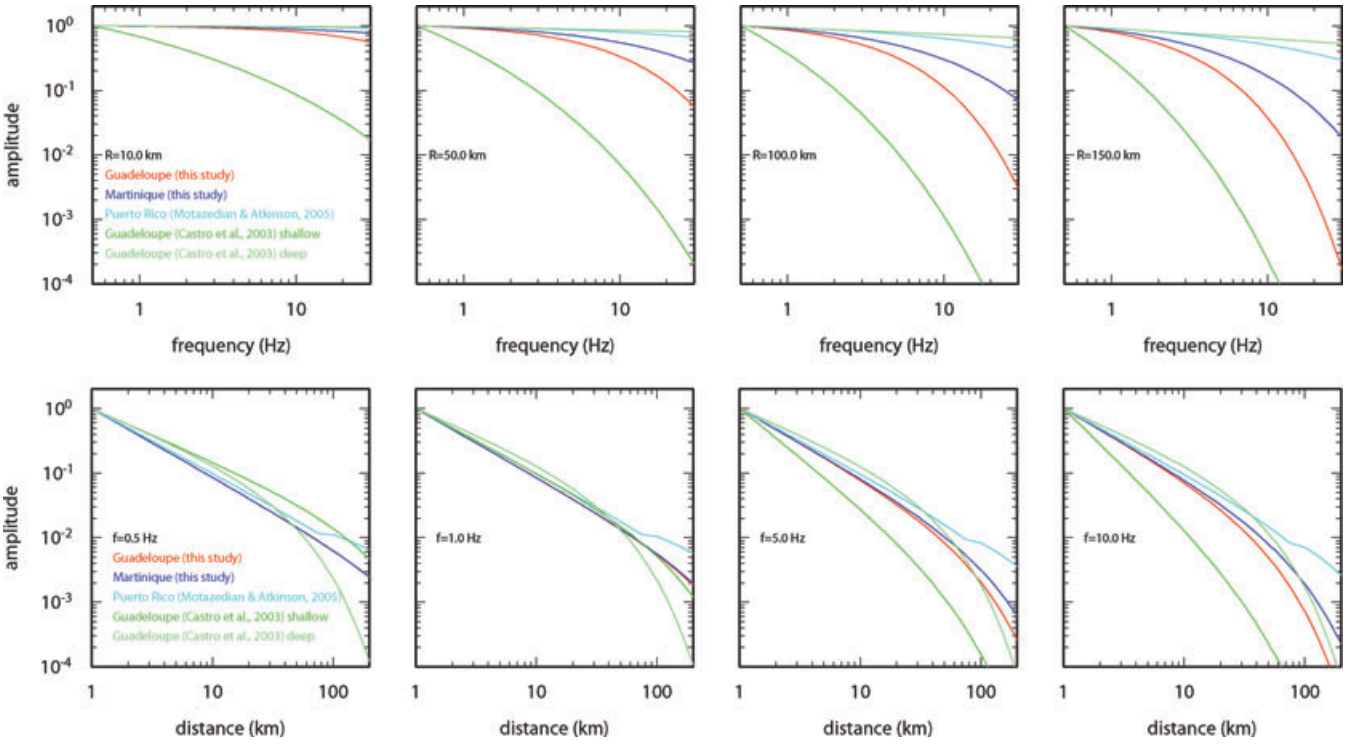

Figure 14. Attenuation models, including both anelastic and geometric attenuation, versus frequency for different distances (top panels), and versus distance for different frequencies (bottom panels). Models for Guadeloupe (red) and Martinique (blue) from this study are shown, as well as the model for Puerto Rico from Motazedian & Atkinson (2005) (cyan), and the model for Guadeloupe from Castro *et al.* (2003) for events with depth lower than 34 km (green) and for events with depth greater than 72 km (light green).

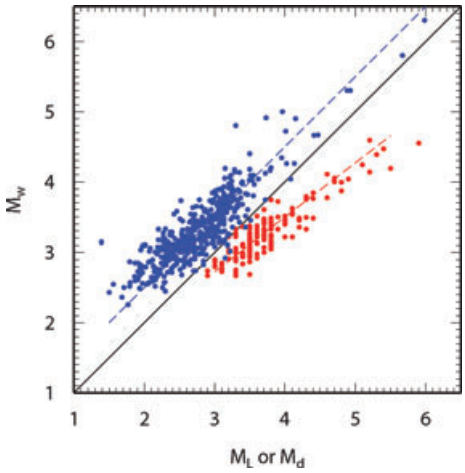

Figure 15. Comparison of inverted M_w versus M_L for French metropolitan area (red) and versus M_d for Guadeloupe (blue). The black line shows the 1:1 relationship.

Inverted site transfer functions have very small standard deviations due to the large number of events recorded at each station. The comparison with H/V ratios from noise recordings shows a good agreement in the resonance frequencies at each station. Moreover, site classification of Douglas (2006) and the results of this work allow the identification of good rock reference sites.

We also determined a path-duration model for the same data, the total duration of ground motion being equal to the sum of the path-duration plus the inverse of the corner frequency. Then, using all the inverted parameters and the path-duration model, we simulate response spectra with the stochastic simulation tool SMSIM (Boore 2003). We used three Brune's stress drop models [(1) inverted stress drops, (2) modelled magnitude-dependent stress drops and (3) average stress drop] and the simulations were performed for the entire data set in each case. Note that in the context of prediction of future ground motions, only the second and third models are useful. The standard deviations of the residuals vary with frequency and range, for the second and third models, between 0.192 and 0.315 (in $\log_{10}$ unit) which are consistent with standard deviations of usual GMPEs (Fig. 17). These results suggest that ground motions from small-to-moderate events are not more variable than those from large events. This apparent magnitude dependence of variability observed in GMPEs (e.g. Youngs *et al.* 1995) results

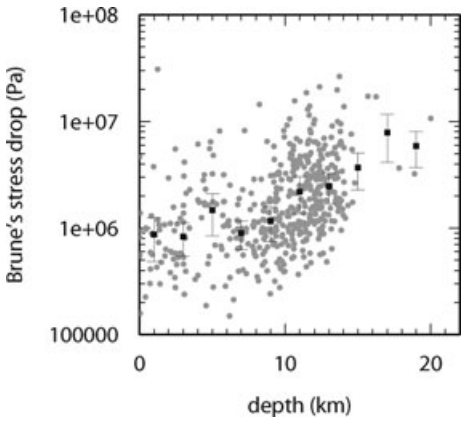

Figure 16. Inverted Brune's stress drops against hypocentral depth (grey dots) and average values over 2 km depth bins (black squares) ± one standard deviation.

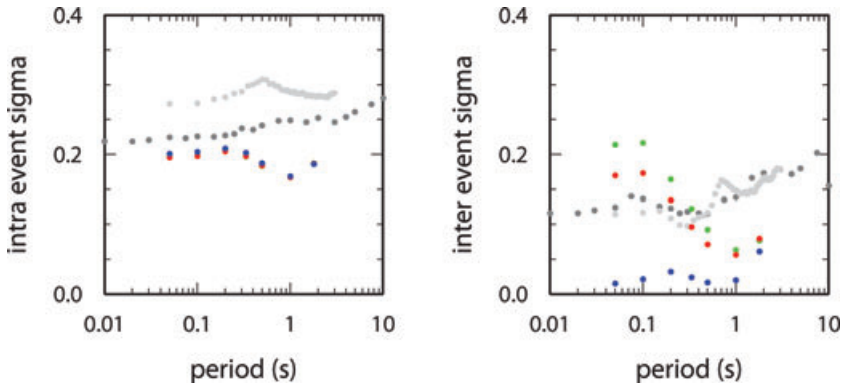

Figure 17. Intra- and interevent standard deviation from Boore & Atkinson (2008) (dark grey), Akkar & Bommer (2010) (light grey) and this study (green: constant stress drop model; red: regressed stress drop model; blue: inverted stress drop).

from greater uncertainty in moment magnitude estimation for smaller events (which is not the case in our study) and could also be a result of an increasing stress drop with magnitude. Fig. 17 shows that the intraevent standard deviations obtained in this study are always lower than those of usual GMPEs. This could be due to the homogeneity of the path analysed since all the events are localized in a small area (close to the single-path assumption). The interevent term suggests that with a good description of the source in terms of moment magnitude but also on its frequency content (i.e. stress drop), this term can be reduced.

We compare our model predictions with those from usual GMPEs, one derived for California (Boore & Atkinson 2008) and one for Europe (Akkar & Bommer 2010). Additionally, a GMPE for PGA derived with data from Guadeloupe and surrounding area is also considered (Beauducel *et al.* 2011). Models are computed for $v_{s30} = 800\ \mathrm{m\,s^{-1}}$. In our case, we used the generic rock profile defined in Cotton *et al.* (2006) after Boore & Joyner (1997) for $v_{s30} = 800\ \mathrm{m\,s^{-1}}$, from which we compute site amplifications. Moreover, a high-frequency decay $\kappa = 0.03$ s is used, consistent with $v_{s30} = 800\ \mathrm{m\,s^{-1}}$ (Van Houtte *et al.* 2011). Predictions for $M_\mathrm{w} = 6.3$ are compared with observations for the main shock, and predictions for $M_\mathrm{w} = 5.0$ and $M_\mathrm{w} = 4.0$ are compared with all the data from earthquakes with M_w in the range 4.9–5.1 and 3.9–4.1, respectively. One has to note that the information on v_{S30} at the stations is not available and we used all the data as if all the stations were located on rock sites. Our predictions are using the magnitude-dependent stress drop model (eq. 16). A factor of 2 is assumed to represent stress drop variability. Note that the uncertainty of the other terms used in the stochastic simulations should be taken into account to properly estimate the variability but we believe they are second order compared to stress drop variability. Fig. 18 compares the data and the models. The two GMPEs Boore & Atkinson (2008) and Akkar & Bommer (2010) are unable to reproduce the steep decay with distance that is observed from data for both the large and small events examples. One has to note that for $M_\mathrm{w} = 4.0$, the GMPEs are used outside their validity range. Our model reproduces the observed amplitudes for all the magnitudes and better captures the distance decay. However, it does not include a near fault saturation term and should consequently not be used for distances less than 10 km.

Finally, our analysis shows that a directivity effect is observable in the data. We could only analyse the largest events in this case due to the lack of focal mechanism determinations for the smaller events. Although directivity is more pronounced for the largest events, it is still observed for some events with magnitude of about 4.5, and our results can help to identify the direction of propagation of the rupture (Fig. 13).

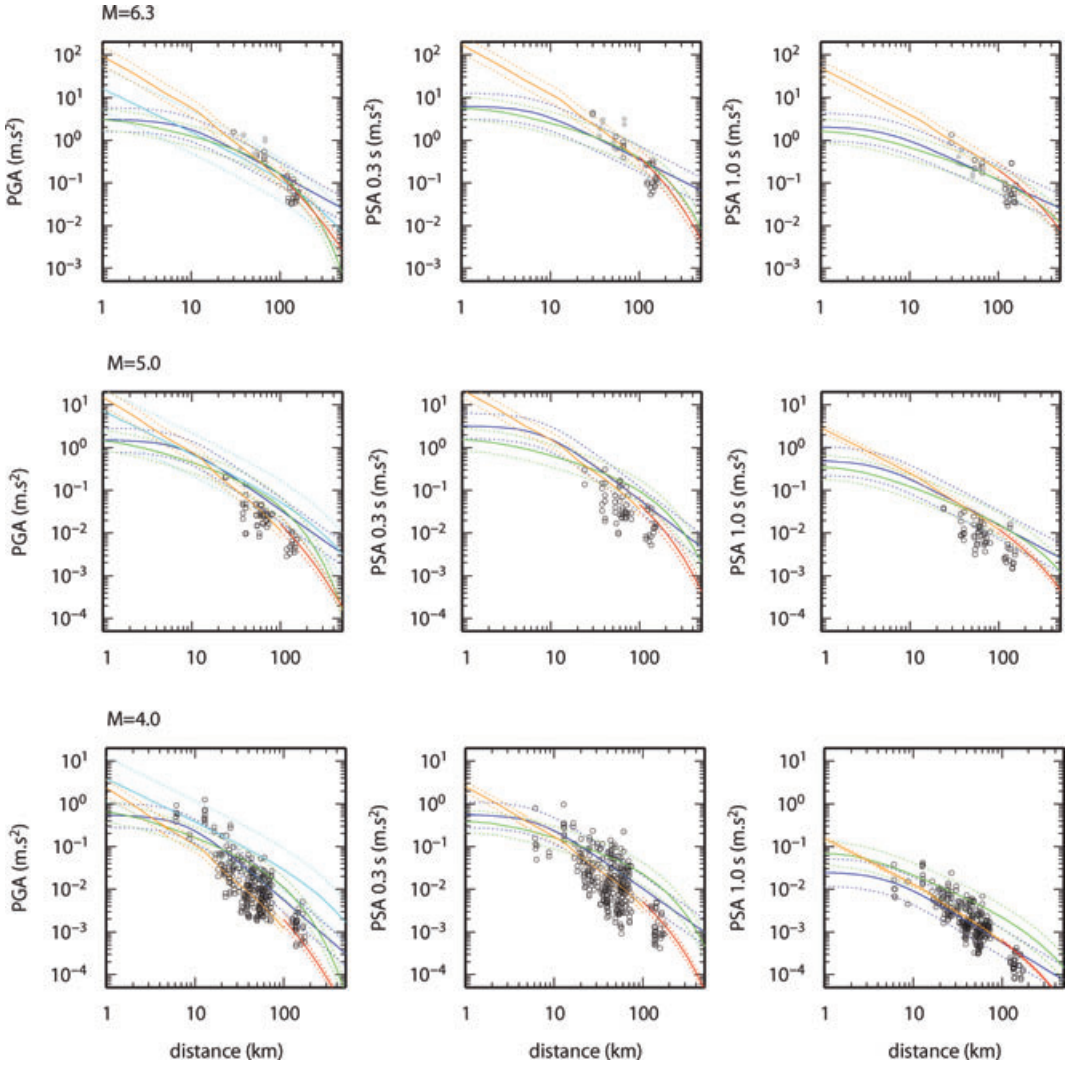

Figure 18. Top panels: data of the $M_w = 6.3$ main shock for PGA (left), PSA at 0.3 s (middle) and PSA at 1.0 s (right) compared with predictions from Boore & Atkinson (2008) (green), Akkar & Bommer (2010) (blue), Beauducel *et al.* (2011) (cyan) and our stochastic models for Guadeloupe (orange) and Martinique (red). Grey data points are related to stations where directivity effects are observed. Middle and bottom panels: Same for $M_w = 5.0$ and 4.0. Note that for $M_w = 4.0$, Boore & Atkinson (2008) and Akkar & Bommer (2010) are used outside their validity range.

ACKNOWLEDGMENTS

The authors would like to thank the Associated Editor Yehuda Ben-Zion and the two anonymous reviewers for their critical and constructive reviews which greatly helped to improve the manuscript. The authors would also like to thank Adrian Rodrigez-Marek (Virginia Tech) for sharing his code to compute random effects as well as Didier Bertil, John Douglas and Agathe Roullé (BRGM) for the H/V data, and Taylor Names, student of the Master in Earthquake Engineering and Engineering Seismology (MEEES) at the University of Grenoble, who helped us to improve English spelling and grammar. This work has been supported by the European Commission through the FP7-ENVIRONMENT-226967 project entitled 'Seismic Hazard Harmonization in Europe' (SHARE) and the FP7-PEOPLE-248182 project entitled 'Ground-motion modelling for seismic hazard assessment in regions with moderate to low seismic activity', and by the French Accelerometric Network (RAP).

REFERENCES

Abercrombie, R.E., 1995. Earthquake source scaling relationships from −1 to 5 M_L using seismograms recorded at 2.5 km depth, *J. geophys. Res.,* **100,** 24 015–24 036.

Abrahamson, N.A. & Youngs, R.R., 1992. A stable algorithm for regression analyses using the random effect model, *Bull. seism. Soc. Am.,* **82**(1), 505–510.

Aki, K. & Richards, P.G., 2002. *Quantitative Seismology,* 2nd edn, University Science Books, Sausalito, CA, 700pp.

Akkar, S. & Bommer, J.J., 2010. Empirical equations for the prediction of PGA, PGV and spectral accelerations in Europe, the Mediterranean region and the Middle East, *Seismol. Res. Lett.,* **82**(2), 195–206.

Andrews, D.J., 1986. Objective determination of source parameters and similarity of earthquakes of different size, in *Earthquake Source Mechanics,* Geophys. Monogr. Ser., Vol. 37, pp. 259–267, eds, Das, S., Boatwright, J. & Scholz, C.H., AGU, Washington, D.C., doi:10.1029/GM037p0259.

Atkinson, G.M. & Boore, D.M., 2006. Earthquake ground-motion prediction equations for Eastern North America, *Bull. seism. Soc. Am.,* **96**(6), 2181–2205.

Atkinson, G.M. & Silva, W., 2000. Stochastic modeling of California ground motions, *Bull. seism. Soc. Am.,* **90**(2), 255–274.

Bay, F., Fäh, D., Malagnini, L. & Giardini, D., 2003. Spectral shear-wave ground-motion scaling in Switzerland, *Bull. seism. Soc. Am.,* **93**(1), 414–429.

Bay, F., Wiemer, S., Fäh, D. & Giardini, D., 2005. Predictive ground motion scaling in Switzerland: best estimates and uncertainties, *J. Seismol,* **9,** 223–240.

Beauducel, F., Bazin, S., Bengoubou-Valerius, M., Bouin, M.-P., Bosson, A., Anténor-Habazac, C., Clouard, V. & de Chabalier, J.-B., 2011. Empirical mode for rapid macroseismic intensities prediction in Guadeloupe and Martinique, *Comptes rendus de l'Académie des Sciences,* in press.

Ben-Zion, Y. & Zhu, L., 2002. Potency-magnitude scaling relations for Southern California earthquakes with $1.0 < M_L < 7.0$, *Geophys. J. Int.,* **148,** F1–F5.

Bengoubou-Valerius, M., Bazin, S., Bertil, D., Beauducel, F. & Bosson, A., 2008. CDSA: a new seismological data center for the French Lesser Antilles, *Seismol. Res. Lett.,* **79**(1), 90–115.

Boatwright, J., Fletcher, J.B. & Fumal, T.E., 1991. A general inversion scheme for source, site, and propagation characteristics using multiply recorded sets of moderate-sized earthquakes, *Bull. seism. Soc. Am.,* **81**(5), 1754–1782.

Bommer, J.J., Stafford, P.J., Alarcón, J.E. & Akkar, S., 2007. The influence of magnitude range on empirical ground-motion prediction, *Bull. seism. Soc. Am.,* **97**(6), 2152–2170.

Boore, D. & Boatwright, J., 1984. Average body-wave radiation coefficients, *Bull. seism. Soc. Am.,* **74**(5), 1615–1621.

Boore, D.M., 2003. Simulation of ground motion using the stochastic method, *Pure appl. Geophys.,* **160,** 635–676.

Boore, D.M. & Atkinson, G.M., 2008. Ground-motion prediction equations for the average horizontal component of PGA, PGV, and 5%-damped PSA at spectral periods between 0.01 and 10 s, *Earthq. Spectra,* **24**(1), 99–138.

Boore, D.M. & Joyner, W.B., 1997. Site amplifications for generic rock sites, *Bull. seism. Soc. Am.,* **87**(2), 327–341.

Brodsky, E.E. & Kanamori, H., 2001. Elastohydrodynamic lubrication of faults. *J. geophys. Res.,* **106**(B8), 16 357–16 374.

Brune, J.N., 1970. Tectonic stress and the spectra of seismic shear waves from earthquakes, *J. geophys. Res.,* **75**(26), 4997–5009.

Brune, J.N., 1971. Correction, *J. geophys. Res.,* **76**(20), 5002.

Castro, R.R., Anderson, J.G. & Singh, S.K., 1990. Site response, attenuation and source spectra of *S* waves along the Guerrero, Mexico, subduction zone, *Bull. seism. Soc. Am.,* **80**(6), 1481–1503.

Castro, R.R., Fabriol, H., Bour, M. & Brun, B.L., 2003. Attenuation and site effects in the region of Guadeloupe, Lesser Antilles, *Bull. seism. Soc. Am.,* **93**(2), 612–626.

Cotton, F., Scherbaum, F., Bommer, J.J. & Bungum, H., 2006. Criteria for selecting and adjusting ground-motion models for specific target regions: application to Central Europe and rock sites, *J. Seismol.,* **10**(2), doi:10.1007/s10950-005-9006-7.

Courboulex, F., Converset, J., Balestra, J. & Delouis, B., 2010. Ground-motion simulations of the 2004 M_w 6.4 Les Saintes, Guadeloupe, earthquake using ten smaller events, *Bull. seism. Soc. Am.,* **100**(1), 116–130.

De Mets, C., Jansma, P.E., Mattioli, G.S., Dixon, T.H., Farina, F., Bilham, R., Calais, E. & Mann, P., 2000. GPS geodetic constraints on Caribbean-North America plate motion, *Geophys. Res. Lett.,* **27**(3), 437–440.

Deng, J. & Sykes, L.R., 1995. Determination of Euler pole for contemporary slip motion of Caribbean and North American plates using slip vectors of interplate earthquakes, *Tectonophysics,* **14**(1), 39–53.

Dixon, T.H., Farina, F., De Mets, C., Jansma, P., Mann, P. & Calais, E., 1998. Relative motion between the Caribbean and North American plates and related boundary zone deformation from a decade of GPS observations, *J. geophys. Res.,* **103**(B7), 15 157–15 182.

Douglas, J., 2006. Errata of and additions to 'Ground motion estimation equations 1964–2003', Intermediary report RP-54603-FR, BRGM, Orléans, France, http://www.brgm.fr/publication/rechRapportSP.jsp (last accessed 2011 June).

Douglas, J., Roullé, A., Dominique, P., Maurin, C. & Dunand, F., 2005. Traitement des données accélérométriques du Conseil Général de la Martinique, Technical report, BRGM, Orléans, France. BRGM/RP-53906-FR.

Douglas, J., Bertil, D., Roullé, A., Dominique, P. & Jousset, P., 2006a. A preliminary investigation of strong-motion data from the French Antilles, *J. Seismol,* **10**(3), 271–299.

Douglas, J., Bungum, H. & Scherbaum, F., 2006b. Ground-motion prediction equations for Southern Spain and Southern Norway obtained using the composite hybrid model perspective, *J. Earthq. Eng.,* **10**(1), 33–72.

Drouet, S., Chevrot, S., Cotton, F. & Souriau, A., 2008. Simultaneous inversion of source spectra, attenuation parameters, and site responses: application to the data of the French accelerometric network, *Bull. seism. Soc. Am.,* **98**(1), doi: 10.1785/0120060215.

Drouet, S., Cotton, F. & Guéguen, P., 2010. v_{S30}, κ, regional attenuation and M_w from small magnitude events accelerograms, *Geophys. J. Int.,* **182**(2), 880–898.

Edwards, B., Rietbrock, A., Bommer, J.J. & Baptie, B., 2008. The acquisition of source, path, and site effects from microearthquake recordings using Q tomography: application to the United Kingdom, *Bull. seism. Soc. Am.,* **98**(4), doi: 10.1785/0120070127.

Feuillet, N., Manighetti, I., Tapponnier, P. & Jacques, E., 2002. Arc parallel extension and localization of volcanic complexes in Guadeloupe, Lesser Antilles, *J. geophys. Res.,* **107**(B12), doi:10.1029/2001JB000308.

Frankel, A., 1991. Mechanisms of seismic attenuation in the crust: scattering and anelasticity in New York State, South Africa, and southern California, *J. Geophys. Res.,* **96**(B4), 6269–6289.

Gagnepain-Beyneix, J., 1987. Evidence of spatial variations of attenuation in the western Pyrenean range, *Geophys. J. R. astr. Soc.,* **89,** 681–704.

Hanks, T.C. & Kanamori, H., 1979. A moment magnitude scale, *J. geophys. Res.,* **84**(B5), 2348–2350.

Ide, S. & Beroza, G.C., 2001. Does apparent stress vary with earthquake size? *Geophys. Res. Lett.,* **28**(17), 3349–3352.

Ide, S., Beroza, G.C., Prejean, S.G. & Ellsworth, W.L., 2003. Apparent break in earthquake scaling due to path and site effects on deep borehole recordings, *Geophys. Res. Lett.,* **108**(B5), 2271, doi:10.1029/2001JB001617.

Konno, K. & Ohmachi, T., 1998. Ground-motion characteristics estimated from spectral ratio between horizontal and vertical components of microtremor, *Bull. seism. Soc. Am.,* **88**(1), 228–241.

Mai, P.M., Spudich, P. & Boatwright, J., 2005. Hypocenter locations in finite-source rupture models, *Bull. seism. Soc. Am.,* **95**(3), 965–980.

Mayeda, K. & Walter, W.R., 1996. Moment, energy, stress drop, and source spectra of western United States earthquakes from regional coda envelopes, *J. geophys. Res.,* **101**(B5), 11 195–11 208.

Motazedian, D. & Atkinson, G., 2005. Ground-motion relations for Puerto Rico, in *Active Tectonics and Seismic Hazards of Puerto Rico, the Virgin Islands, and Offshore Areas,* pp. 61–80, ed. Mann, P., Geological Society of America Special Paper 385.

Oth, A., Bindi, D., Parolai, S. & Giacomo, D.D., 2011. Spectral analysis of K-NET and KIK-net data in Japan, Part II: on attenuation characteristics, source spectra, and site response of borehole and surface stations, *Bull. seism. Soc. Am.,* **101**(2), 667–687.

Pequegnat, C., Guéguen, P., Hatzfeld, D. & Langlais, M., 2008. The French Accelerometric Network (RAP) and National Data Center (RAP-NDC), *Seismol. Res. Lett.,* **79**(1), 79–89.

Prejean, S. & Ellsworth, W.L., 2001. Observations of earthquake source parameters at 2 km depth in the Long Valley Caldera, eastern California, *Bull. seism. Soc. Am.,* **91**(2), 165–177.

Radiguet, M., Cotton, F., Manighetti, I. & Campillo, M., 2009. Dependency of near-field ground motions on the structural maturity of the ruptured faults, *Bull. seism. Soc. Am.,* **99**(4), 2572–2581.

Raoof, M., Herrmann, R.B. & Malagnini, L., 1999. Attenuation and excitation of three-component ground motion in southern California, *Bull. seism. Soc. Am.,* **89**(4), 888–902.

Scherbaum, F., Cotton, F. & Smit, P., 2004. On the use of response spectral-reference data for the selection and ranking of ground-motion models

for seismic-hazard analysis in regions of moderate seismicity: the case of rock motion, *Bull. seism. Soc. Am.,* **94**(6), 2164–2185.

Tarantola, A., 2004. *Inverse Problem Theory and Methods for Model Parameters Estimation,* SIAM, Philadelphia, PA.

Van Houtte, C., Drouet, S. & Cotton, F., 2011. Analysis of the origins of κ (Kappa) to compute hard rock to rock adjustment factors for GMPEs, *Bull. seism. Soc. Am.,* **101**(6), doi:10.1785/0120100345.

Walter, W.R., Mayeda, K., Gok, R. & Hofstetter, A., 2006. The scaling of seismic energy with moment: simple models compared with observations, in *Earthquakes: Radiated Energy and the Physics of Faulting,* Geophys. Monogr. Ser., Vol. 170, pp. 25–41, eds, Abercrombie, R., McGarr, A., Kanamori, H. & Di Toro, G., AGU, Washington, D.C.

Youngs, R.R., Abrahamson, N.A., Makdisi, F.I. & Sadigh, K., 1995. Magnitude dependent variance of peak ground acceleration, *Bull. seism. Soc. Am.,* **85**(4), 1161–1176.

SUPPORTING INFORMATION

Additional Supporting Information may be found in the online version of this article:

Table S1. Earthquakes analysed in this study. Date, localization and duration magnitude (M_d) are from the OVSG. The recording distance range is also indicated as well as the moment magnitudes, corner frequencies and stress drops determined in this study.

Please note: Wiley-Blackwell are not responsible for the content or functionality of any supporting materials supplied by the authors. Any queries (other than missing material) should be directed to the corresponding author for the article.